Research Paper

Fabrication and Characterization of Polysulfone/Iron Oxide Nanoparticle Mixed Matrix Hollow Fiber Membranes for Hemodialysis: Effect of Dope Extrusion Rate and Air Gap

Noresah Said [1], Sumarni Mansur [1], Muhammad Nidzhom Zainol Abidin [2,3,*], Ahmad Fauzi Ismail [1]

[1] Advanced Membrane Technology Research Centre, Universiti Teknologi Malaysia, 81310 Johor Bahru, Malaysia
[2] Department of Chemistry, Faculty of Science, Universiti Malaya, 50603 Kuala Lumpur, Malaysia
[3] Chemistry Department, Faculty of Science and Technology, Universitas Airlangga, Surabaya 60115, Indonesia

Article info

Keywords
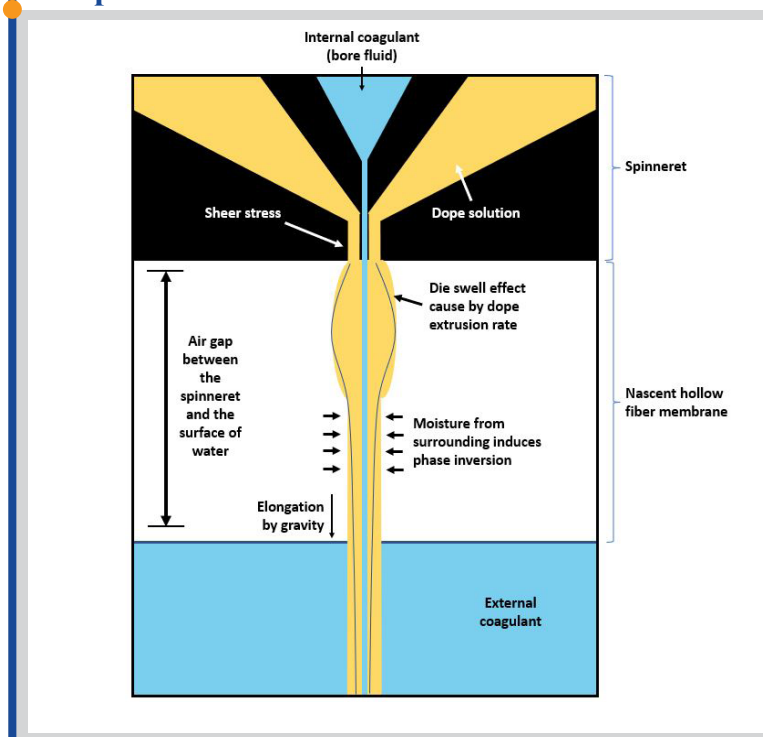
Highlights

- PSf/Fe$_2$O$_3$ mixed matrix HFMs are prepared via the dry-wet spinning technique
- DER and air gap influence the HFMs' morphology and liquid separation performance
- Ideal morphology for hemodialysis is obtained at the optimum DER and air gap
- Desired permeability and selectivity are achieved at the optimum DER and air gap

Graphical abstract

Abstract

Membrane fabrication aspects include the membrane formulation and composition, the operating parameter, and the proper condition during membrane spinning which affect the membrane morphology. In this study, mixed matrix hollow fiber membranes (HFMs) which are composed of polysulfone (PSf) and iron oxide nanoparticles, Fe$_2$O$_3$, were developed with the focus on investigating the effects of dope extrusion rate (DER) and air gap on the morphological properties and the liquid separation performance of the mixed matrix HFMs for hemodialysis application. The mixed matrix HFMs were fabricated via dry-wet spinning technique at various DER (1.0, 1.5, 2.0, and 2.5 mL/min) and air gaps (10, 30, 40, 50, and 60 cm), followed by the morphological characterization and the permeation study of the mixed matrix HFMs. At the DER of 1.0 mL/min and the air gap of 50 cm, the mixed matrix HFMs displayed the most ideal morphology. Furthermore, the mixed matrix HFMs attained the pure water permeability of 70.84 Lm^{-2}h^{-1}bar^1, the bovine serum albumin rejection of 98.2%, and the optimum molecular sieving profile. The effects of DER and air gap heightened the morphological properties and the liquid separation performance of PSf/Fe$_2$O$_3$ mixed matrix HFMs for hemodialysis application

1. Introduction

End-stage renal patients depend on hemodialysis treatment for their day-to-day well-being [1–3]. The treatment ensures intoxicated blood is purified before returning to the human blood circulatory system. The method of blood purification utilizes semi-permeable membranes in order to mimic the function

of the kidney for the removal of uremic toxin molecules. This principle includes simple diffusion, dialysis, convection, and ultrafiltration [4,5]. Blood passes through a module filled with the hollow fiber membrane (HFM) in one direction while the dialysate, i.e., the mixture of pure water, electrolyte, and salts pass through in the opposite direction of the blood flow [6]. The difference in flow between blood and the dialysate creates a counter-current flow gradient that enables the separation process to happen [7].

The success of the hemodialysis treatment majorly depends on the HFM in removing uremic toxins molecules and retaining essential proteins in blood [8]. The preparation of HFM specifically designed for specific applications is a complex process. In membrane separation, the morphology of the membrane plays important role in achieving high flux and excellent solute removal. Normally, the fabrication technique would contribute to the tailoring of the morphology and the effect is a lot more prominent for hollow fiber configuration. Besides, the fabrication of the HFMs involves more complex controlling parameters such as length of the air gap, bore fluid composition, and dope extrusion rate (DER) as compared to flat sheet membranes [9,10].

In the past decades, many studies investigated the influence of various controlling parameters in the spinning process [11,12]. The process starts when the polymer is extruded out of a channel in a spinneret orifice, where the shear stress that has been induced within the spinneret dramatically affects the molecular orientation and the relaxation of the polymer across the nascent HFM [13]. In a study by Korminouri [14], air gaps played a crucial part in tailoring membrane morphology to improve the membrane separation performance. An air gap, which determines the time taken before a dope solution reaches the coagulation bath affects the polymer molecular orientations and molecular relaxation. It also induces the strain outside the spinneret caused by the gravity and the spin line stress which made the kinetics and the dynamics of phase inversion processes complicated [15].

Moreover, the effect of DER has also been investigated by many researchers [11,16,17]. DER is believed to affect shear stress during the fabrication of HFMs, where it was found to change the degree of molecular orientation which majorly affects the formation of the membrane skin layer [17]. This phenomenon resulted in the alteration of membrane morphology and eventually affected membrane separation performance.

Nevertheless, the influence of varying the air gap on the mixed matrix HFM morphological properties and liquid separation performance, as reported in previous studies showed contradicting results. No study has deeply investigated the effect of different air gaps in the context of hemodialysis membranes. Furthermore, previous studies regarding the effect of DER on membrane morphology and separation performance were mostly revolving around the neat membrane only and contradicting among different polymer materials. Thus, the data recovered based on only the neat membrane composition of any particular material can be misleading when it comes to developing a nanocomposite membrane. The addition of nanoparticles in the membrane was proven to change the rheological properties of the dope solution due to their interaction with the polymer [18–20]. The size of nanofillers and their distribution in the membrane matrix can also affect the membrane properties.

Nanoparticles based on metal and metal oxide have been employed in many membrane separation processes to offer their hydrophilic property and high surface area for better membrane pore interconnectivity with increased porosity. Iron oxide nanoparticle, Fe_2O_3, is an example of a metal oxide having the ideal attributes, i.e., biocompatible and low toxicity, to be incorporated in hemodialysis membranes [21].

In our previous work, we investigated the influence of air gap on the morphology of the neat polysulfone (PSf) membrane [22]. We successfully showed that a higher air gap significantly influences the permeability of the membrane. However, the addition of nanofillers in a dope solution could have changed the rheological properties of the solution and thus affect the sheer rate during the phase inversion process. Hence, this work aims to investigate the effects of different DERs and air gaps on the morphological properties and the toxin removal performance of PSf mixed matrix HFMs incorporated with Fe_2O_3. The outcomes of this study include a better understanding of the impact of DER and air gap in tailoring the morphological structure of PSf/Fe_2O_3 mixed matrix HFMs and how these two parameters would affect the membrane performance. Finally, the most suitable DER and air gap for the ideal morphology of the PSf/Fe_2O_3 hemodialysis membrane could be determined.

2 Experimental

2.1 Materials

PSf polymer (69.5 kDa) was obtained from Solvay Advanced Polymers (Malaysia), polyvinylpyrrolidone (PVP, 360,000 g/mol), and citric acid (192.12 g/mol) were supplied from Sigma Aldrich and were used as additives

and surfactant, Fe_2O_3 were obtained from Nova Scientific and were used as nanofillers (size= 20 nm). *N*-methyl-2-pyrrolidone (NMP, 98%) was used as the solvent, and glycerol (92.1 g/mol) was used for membrane post-treatment, both chemicals obtained from Merck.

Poly(methyl methacrylate) (PMMA) tube was used as the membrane module housing together with the Loctite E-30CL Hysol® as the epoxy glue. Urea, creatinine, homocysteine, lysozyme, and bovine serum albumin (BSA) were supplied by Sigma Aldrich.

2.2 Fabrication of PSf/ Fe₂O₃ mixed matrix HFMs

The dope solution which comprises 18 weight percent (wt%) PSf, 4.8 wt% PVP, 0.1 wt% Fe_2O_3, and 2 wt% citric acid in NMP was prepared. The dry-wet spinning technique was used to fabricate the mixed matrix HFMs. The dope solution, pressured by N_2, was channeled into a spinneret with the outer diameter (OD)/inner diameter (ID) of 0.8/0.4 mm by a gear pump. The temperature of the bore fluid (reverse osmosis water) and the coagulation bath (tap water) was maintained at 25 °C. The DER and the bore fluid flow rate ratio was maintained at 1:1. During the spinning process, the DER was varied at 1.0 mL/min (D1), 1.5 mL/min (D2), 2.0 mL/min (D3) and 2.5 mL/min (D4), while maintaining 10 cm air gap between the spinneret and the water surface. After obtaining the optimum DER, the air gap was varied at 10 cm, 30 cm, 40 cm, 50 cm, and 60 cm, and the fabricated membranes were labeled as A10, A30, A40, A50, and A60, respectively. The membrane fibers were collected at the rate of 10 m/min. The spun membranes were immersed in 10 wt% glycerol solution for 48 hours.

2.3 Mixed matrix HFM characterization

The outer surfaces and cross-sections of all membranes were examined using scanning electron microscopy (SEM, Hitachi Table Top TM3000). Before the analysis, the prepared mixed matrix HFMs samples were sputter-coated with gold. Besides, the membrane surface wettability was evaluated using a contact angle goniometer (Krüss Gambult, Germany). In addition, the porosity and the pore size of the mixed matrix HFMs were measured by the dry-wet weighing method and the filtration velocity method, respectively [23]. The membrane fibers (10 pieces x 5 cm) were equilibrated in water for 240 mins before they were dried. The membrane porosity, ε was calculated using Eq. (1):

$$\varepsilon = \frac{(W_{wet} - W_{dry})}{V_{\rho w}} \times 100\% \tag{1}$$

where ε is the membrane porosity (%), W_{wet} is the mass of the wet membrane, W_{dry} is the mass of the dry membrane, V is the membrane volume and ρw is the water density. The average pore radius, r (m) was calculated using Eq. (2):

$$r = \sqrt{\frac{2.9 - 1.75\varepsilon \times 8\eta l Q}{\varepsilon \times A \times \Delta P}} \tag{2}$$

where η represents the water viscosity at 25 °C, l represents the membrane thickness (m), Q represents the volume of the permeate water per unit time (m^3/s), A represents the effective surface area of the membrane (m^2) and ΔP represents the operating pressure (Pa). From the r-value, the diameter of the pores was determined.

2.4 Crossflow ultrafiltration (UF) experiments

The membrane separation features were assessed in terms of PWP and albumin rejection using a crossflow UF system, as shown in Fig. 1. The membrane modules (25 cm x 1.3 cm) packed with 60-65 fibers of mixed matrix HFMs were prepared and before measurement, they were pressurized at the transmembrane pressure (TMP) of 1 bar for 30 min.
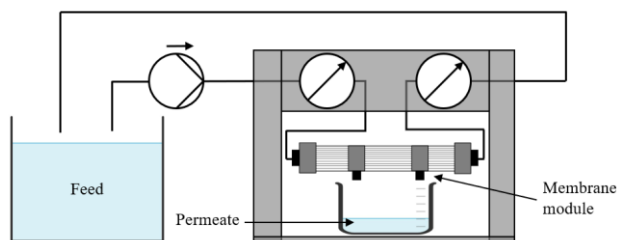

Fig. 1. Experimental setup for the UF experiment.

2.4.1 Pure water permeability (PWP) and BSA rejection

To determine the PWP, the membrane module was fed with water at the TMP of 0.7 bar, which was within the normal range of TMP during hemodialysis [24,25]. The PWP, P_w (Lm^{-2}h^{-1}bar^{-1}) was evaluated using Eq. (3) [23]:

$$P_w = \frac{V}{A \times \Delta t \times \Delta P} \tag{3}$$

where V represents the permeate volume (L), A represents the effective surface area (m^2), Δt represents the permeation time (h) and ΔP represents the TMP. Next, the membrane module was fed with 500 ppm BSA solution at the TMP of 0.7 bar. The concentration of BSA in the feed and the permeate was determined using the UV-vis spectrophotometer (Hach, DR5000, Canada). The BSA rejection of the mixed matrix HFMs was then evaluated.

2.4.2 Sieving coefficient (SC)

The membrane SC was also determined using the crossflow UF setup. The following compounds were separately dissolved in reverse osmosis water with the initial concentration of 1500 ppm urea (60 Da), 100 ppm creatinine (112 Da), 100 ppm homocysteine (135 Da), 400 ppm lysozyme (14 kDa) and 1000 ppm BSA (67 kDa). The solutions were then fed into the membrane module at the TMP of 0.7 bar. The concentrations of homocysteine, lysozyme and BSA in their respective permeates were analyzed using the UV-vis spectrophotometer at the scanning wavelength of 180 nm, 280 nm, and 278 nm, respectively. In the case of urea and creatinine, their concentrations in permeate were detected using Quanti-Chrom™ Urea Assay Kit and Quanti-Chrom™ Creatinine Assay Kit, respectively. The SC was calculated using Eq. (4):

$$SC = \frac{C_p}{C_f} \tag{4}$$

where C_p represents the compound concentration in permeate and C_f represents the compound concentration in the feed. SC=1 signifies that the compound freely passes through the membrane while SC=0 signifies that the membrane rejects the compound completely.

3 Results and discussion

3.1 Effect of DER on the membrane morphology

In most cases, the formation of different membrane structures, i.e., porous and dense structures, depends on the rate of solvent/non-solvent exchange involved during the phase inversion process to form the membrane. The non-solvent is represented by the bore fluid and the coagulation bath. A dense structure is formed by the rapid solvent/non-solvent exchange. The finger-like structure which is an example of a porous structure is the follow-through section coming from the dense structure due to the slightly delayed phase inversion. Another porous structure namely a sponge-like structure is formed at a much slower rate of solvent/non-solvent exchange.

The cross-sectional images of PSf/Fe$_2$O$_3$ mixed matrix HFMs spun at different DER are displayed in Fig. 2. Except for membrane D4, all membranes have asymmetrical structures with a dense selective layer and a porous sublayer. The long finger-like structure was created from the membranes' inner side, while the sponge-like structure spanned towards the outer side of the membranes. The most obvious effect of DER was shown by the thickness of the membrane's outermost layer. At higher DER, the sponge layer became thicker and denser. Upon extruding through the spinneret, the polymer chains aligned themselves closer at higher DER which has led to a more compact sponge-like structure [26].
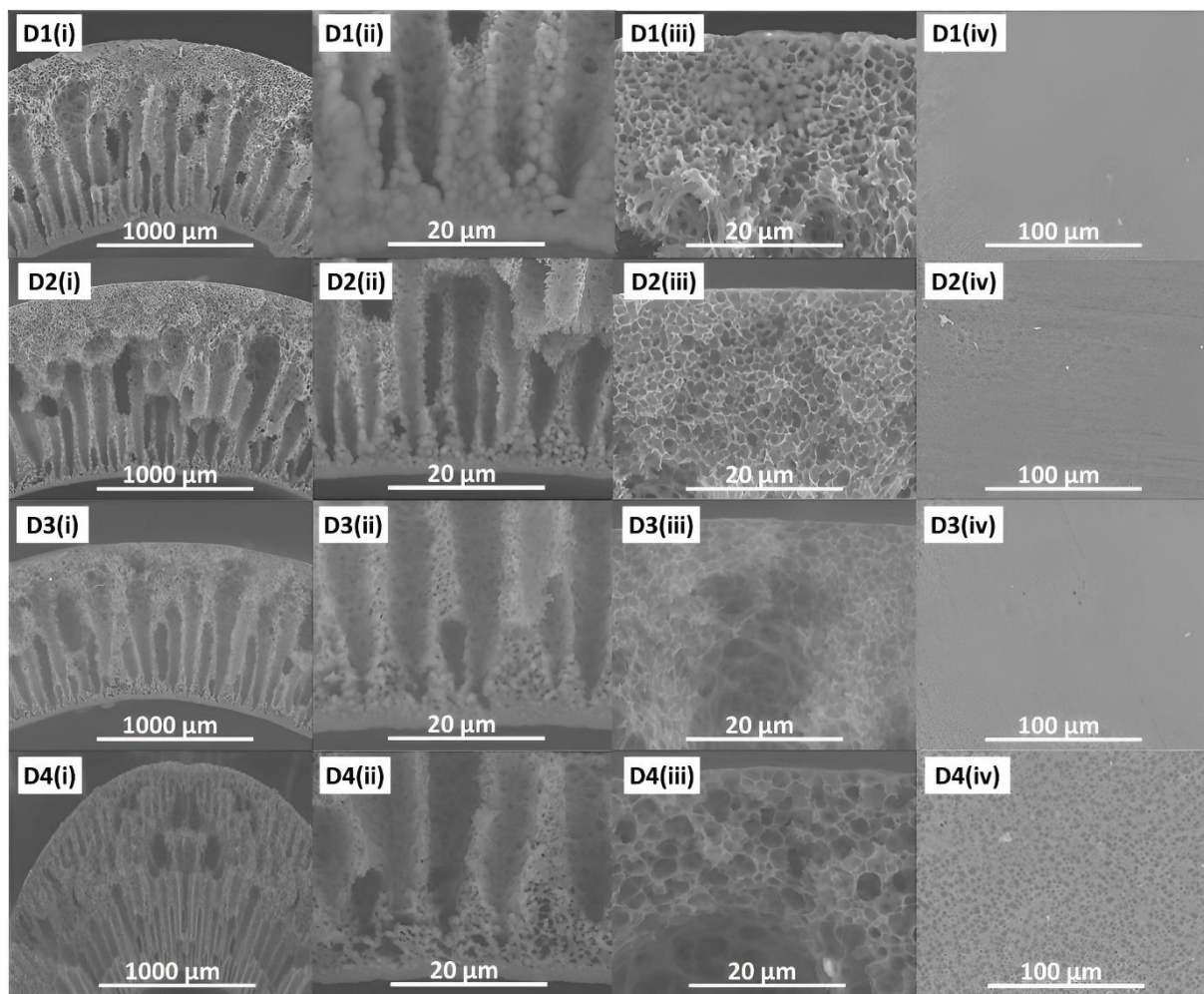
Fig. 2. The SEM images of membrane D1, membrane D2, membrane D3, and membrane D4: (i) cross-sectional images at 1000x magnification, (ii) outer region of the cross-sectional images at 4000x magnification, (iii) inner region of the cross-sectional images at 4000x magnification, (iv) surface images at 1000x magnification.

On the other hand, the inner skin layer of the membranes possessed a dense structure regardless of the DER used. Water as the bore fluid has rendered fast polymer precipitation that took place during the spinning process. The SEM images of membrane D4 show the formation of an irregular sandwich-like structure. The rheological properties of the dope solution caused stress created from the rapid solvent exchange [17]. This morphology is not suitable for hemodialysis as the membrane would cause a more severe protein entrapment inside the polymer matrix which can render the decrease in membrane transport properties due to irreversible fouling.

At the outer surface, the membrane structure appeared to be denser at faster DER up to 2.0 mL/min. The pore size became smaller as the DER increased due to the stronger force acted on the membrane structure. However, the pore at the outer surface of membrane D4 was the biggest. Due to the reduced residence time as the result of faster DER, the evaporation of solvent to the air was limited. This allowed the complete phase inversion of the membrane outer surface to occur inside the external coagulation bath. The demixing between solvent and water created larger pores at the outer surfaces of the membrane as compared to the membranes exposed towards longer evaporation-induced phase inversion process.

The dimensional changes of the membrane spun at different DER are shown in Table 1. The changes in the volume of dope solution extruded from the spinneret per unit of time have changed the dimension of the membrane. Both OD and ID of the membrane were increased with the increasing DER. Besides that, the membrane wall was also significantly thickened with increasing DER. According to Peng *et al.* [17], this phenomenon happened due to the "Barus effect", where the polymer stream was compressed into the spinneret and then partially recovered to the former shape once extruded out of the spinneret.

Table 1
Dimensional changes of PSf/Fe$_2$O$_3$ mixed matrix HFMs at different DERs.

DER (mL/min)	OD (µm)	ID (µm)	OD/ID Ratio	Wall Thickness (µm)
1.0	420	300	1.40	60
1.5	550	410	1.34	70
2.0	620	420	1.48	100
2.5	890	490	1.82	200

Based on the morphology of the membranes as the result of manipulating the DER, it can be deduced that the lower DER was more suitable to fabricate a small dimension HFM. In this study, the lowest DER used was 1.0 mL/min. The dimension of the membrane was comparable to that of commercial hemodialysis membranes [27]. A smaller membrane may provide a larger surface area for more efficient separation and a thinner wall could minimize the resistance for mass transfer.
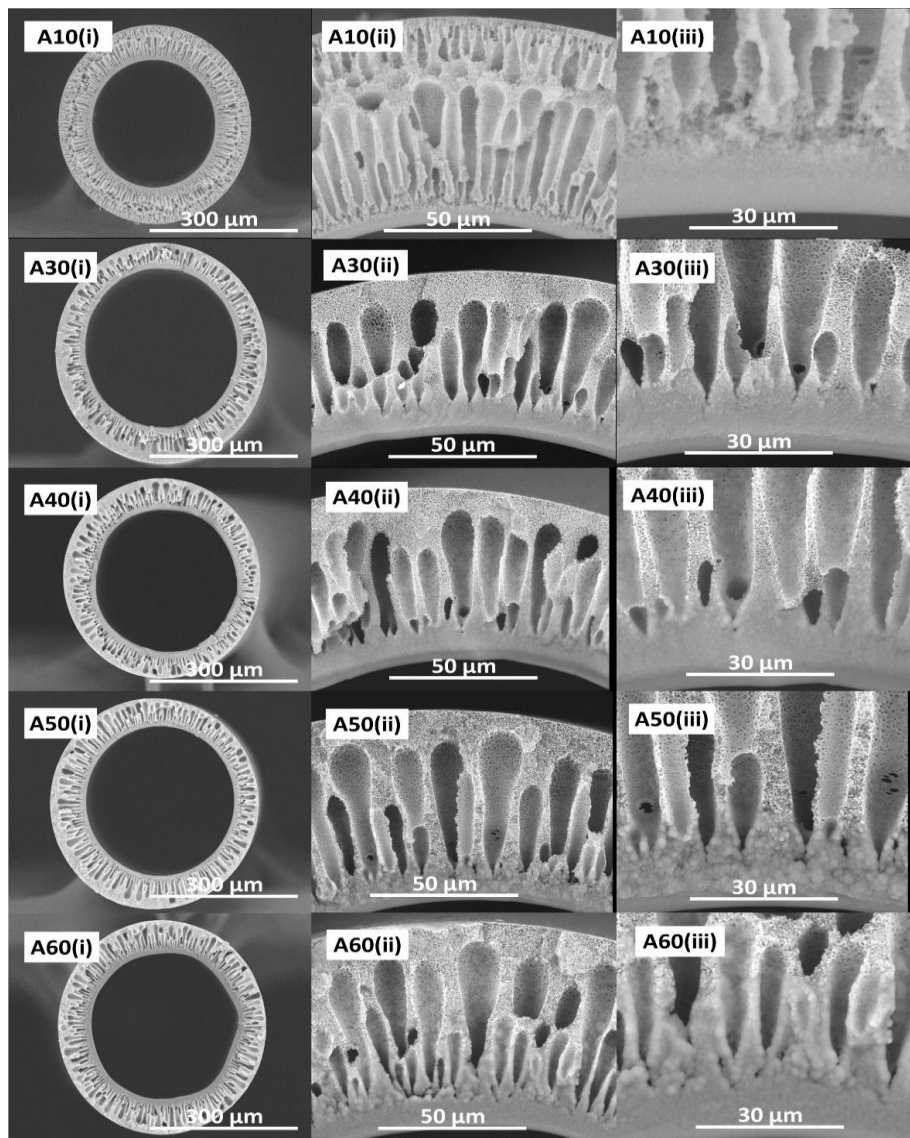
Fig. 3. The SEM cross-sectional images of membrane A10, membrane A30, membrane A40, membrane A50, and membrane A60: (i) cross-sectional images at 150x magnification, (ii) cross-sectional images at 1000x magnification, (iii) inner region of the cross-sectional images at 4000x magnification.

3.2 Effect of air gap on the membrane morphology

SEM images of PSf/Fe$_2$O$_3$ mixed matrix HFMs spun at the air gap from 10 to 60 cm are shown in Fig. 3. Excluding membrane A10, the membranes have an asymmetric structure. Membrane A10 showed a sandwich-like structure, made up of two dense layers and two rows of finger-like structures, one with a longer and bigger void than the other. At a lower air gap (< 30 cm), the solvent-moisture exchange did not happen at the membrane's outer surface since the residence time in the air (dry spinning) was brief. Instead, the inner and outer sides of the membrane instantaneously solidified. The prompt precipitation at both sides of the membrane produced the two dense selective layers with an array of finger-like structures each.

Nevertheless, membranes spun at the air gap 30 to 60 cm possessed one array of finger-like structures and a sponge-like structure at the membranes' outermost region due to the evaporation of NMP during the dry spinning. The dense selective layer was formed by the instantaneous solvent/non-solvent exchange at the innermost region [28]. The obtained morphologies fulfilled the membrane properties for hemodialysis, whereby the nano-sized pores at the membrane's inner surface could prevent clogging by large proteins [29]. Furthermore, the tiny pores at the selective layer can retain albumin while allowing uremic toxins to cross the membrane.

From Fig. 3, the pore size at the membrane outer region increased with the increasing air gap. This was due to the moisture-induced phase inversion taking place at the membrane's outer surface at the higher air gap (> 30 cm). The longer the residence time in the air, the bigger the pore size. In a delayed phase inversion, the polymer may have more time to nucleate into larger pores. Sometimes, two or more pores converge to create one bigger pore. In hemodialysis, the large pore size can facilitate the movement of large uremic toxins across the membrane.

In membrane separation processes, the dimension of a membrane, for instance, the wall thickness becomes one of the factors influencing the hydraulic permeability of the membrane [28]. A thicker membrane wall would increase the resistance toward the solutes and water molecules. The dimensional changes of the membranes spun at different air gaps are shown in Table 2. The air gap plays a very important role in tailoring the membrane dimension. Based on the measurement, both OD and ID of the membrane reduced with the increasing air gap. The larger air space after the dope solution extruded from spinneret and before the HFM reaches the external coagulation bath has exposed the membrane in its nascent state to external forces. The polymer molecular chain and the bore fluid experienced the thinning effect after both being pulled by gravitational force. However, the membrane wall became slightly thicker as the air gap was increased from 30 cm onwards after experiencing a significant reduce of thickness from 116 to 67 µm.

Table 2
Dimensional changes of PSf/Fe$_2$O$_3$ mixed matrix HFMs at different air gaps.

Air gap (cm)	OD (µm)	ID (µm)	OD/ID ratio	Wall thickness (µm)
10	645	413	1.56	116
30	482	348	1.39	67
40	477	342	1.40	68
50	474	334	1.42	70
60	468	323	1.45	73

3.2.1 PSf/Fe$_2$O$_3$ mixed matrix HFMs pore size and porosity

The mixed matrix HFMs pore size and porosity are shown in Fig. 4. The membrane displayed a significant increase in average pore size with the increasing air gap. The higher the air gap, the longer the duration of gravitational pull imposed on the membrane, hence producing a membrane with bigger pores [10,14]. The polymer macromolecules also experienced swelling and relaxation from the beginning of the extrusion from the spinneret. The shifting of the macromolecule orientation in the membrane induced the formation of a larger average pore size.

Meanwhile, the membrane prepared at a 50 cm air gap was the most porous, as shown in Fig. 4. Based on the line graph, there was a slight increase in the porosity from membrane A10 to membrane A30, and after that a substantial increment until membrane A50. The stronger elongation stress during spinning due to the higher air gap has pulled the polymer chains apart and subsequently created voids. Consequently, the membrane-free volume was increased. The increase in free volume allowed the bore fluid to easily penetrate the polymer matrix and eventually led to faster solvent-water exchange. Due to the rapid phase inversion, a longer and bigger finger-like structure was formed. On the contrary, the unfavorable change in the polymer orientation due to the weak force imposed on the membrane prepared at a lower air gap has caused a decrease in membrane porosity [30].
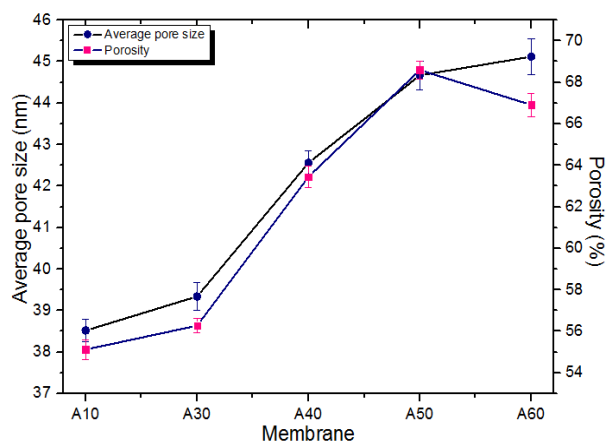
Fig. 4. Average pore size and porosity of PSf/Fe$_2$O$_3$ mixed matrix HFMs at different air gaps.

3.2.2 Water contact angle analysis

Surface hydrophilicity is an important feature for hemodialysis membranes to minimize protein adsorption, which is the first thing that initiates the inflammatory interactions between membrane and blood, hence leading to undesirable results. Fig. 5 shows the membranes' hydrophilicity measured using a contact angle goniometer. The water contact angle revealed that the mixed matrix HFMs depicted a smaller contact angle with the increasing air gap. Membrane A60 exhibited the smallest contact angle which is 51.7°, showing significant hydrophilicity improvement compared to the membrane spun at the lowest air gap (membrane A10). The trend showing improved surface hydrophilicity with air gap was expected. The same effects that happened to the membrane morphology, i.e., changes in dimension, porosity, and pore size due to the increasing air gap have caused the membrane surface more permeable to water molecules [15].
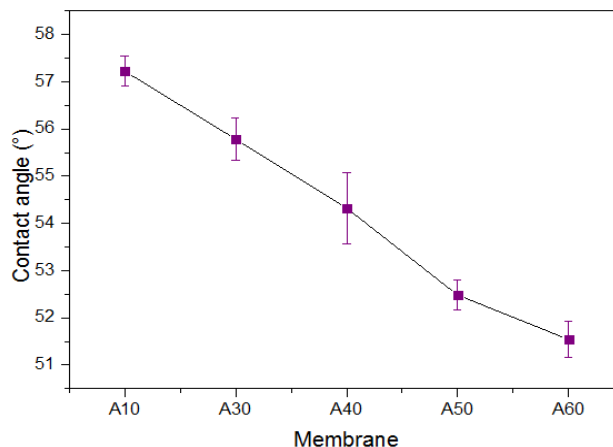
Fig. 5. Contact angle of the PSf/ Fe$_2$O$_3$ mixed matrix HFMs at different air gaps.

3.2.3 Results of PWP and BSA rejection

The PWP and BSA rejection of membranes spun at different air gaps are shown in Fig. 6. Membrane A10 exhibited a very low PWP due to its dual-selective layer morphology with tiny pores. Significant improvements in PWP were reported as the air gap was increased until the PWP achieved its highest value at 50 cm air gap (70.84 Lm^{-2}h^{-1}bar^{-1}). The longer and larger finger-like structure of the membrane promoted the movement of water. On top of that, the increased porosity of the membranes fabricated at higher air gaps has improved the PWP by the membrane's capacity to equilibrate more water molecules at one time. The improved PWP is a good indication, whereby the membrane possesses a better chance to remove middle molecular uremic toxins by convection.
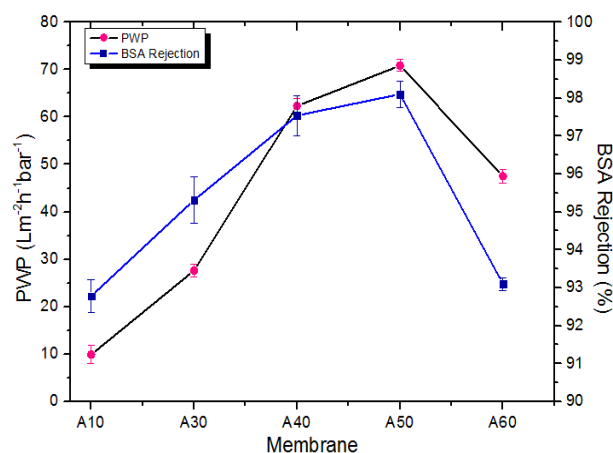
Fig. 6. The PWP and BSA rejection of the PSf/ Fe$_2$O$_3$ mixed matrix HFMs at different air gaps.

Fig. 7. Sieving profiles of PSf/Fe$_2$O$_3$ mixed matrix HFMs.

Meanwhile, all membranes achieved sufficient BSA rejection of greater than 90% to prevent albumin loss during hemodialysis treatment [31]. The tight arrangement of nanopores at the dense selective layer of the membrane has limited the passage of BSA molecules through the membranes. These findings proved that membrane separation characteristics could be affected by the changes in membrane morphology as the result of applying different air gaps. Moreover, it was found that the BSA rejection increased with the increasing PWP, most probably due to the improved routes for water molecules. At the same time, the large BSA molecules were left behind. Although the increasing hydrophilicity was not prominent, the interaction between the membrane surface and the hydrophobic BSA became weaker.

Meanwhile, the decreasing performance of membrane A60 somehow corresponded to its morphology as discussed before. The formation of a thicker wall has now caused stronger resistance for water molecules to pass through the membrane. Moreover, the slight reduction of BSA rejection could be explained by the increased average pore size [20].

3.2.4 Sieving curve

To achieve an excellent hemodialysis process, the membrane must selectively remove a wide range of uremic toxins while keeping the essential proteins in the blood. Fig. 7 presents the sieving curves of the PSf/Fe$_2$O$_3$ mixed matrix HFMs fabricated at various air gaps. Generally, the membranes spun at the higher air gap displayed a sharper sieving curve. Membrane A50 had the best SC values: 1 for urea (60 Da) and creatinine (112 Da); 0.94 for homocysteine (135 Da); 0.71 for lysozyme (14, 000 Da) and 0.03 for BSA (66, 000 Da). The high SC value for lysozyme was an excellent indicator to attain a high removal of middle molecular toxins during hemodialysis [32]. Based on the finding, it can be suggested that the membrane fabricated at a 50 cm air gap possessed excellent selectivity for hemodialysis.

4. Conclusion

A systematic investigation on the influence of two spinning parameters which are DER and air gap towards PSf/Fe$_2$O$_3$ mixed matrix HFMs has been conducted. The major effects that have been investigated were the morphological properties and the liquid separation characteristics of the HFMs. Morphological results showed that an increase of DER during the membrane spinning process increased the dimension of the fiber along with the increase in thickness of the membrane wall. Approaching the DER of 2.5 mL/min, the membrane turned into an irregular sandwich-like structure. It appeared that the lowest DER (1.0 mL/min) produced the most suitable membrane morphology for hemodialysis. On the contrary, the increase in the air gap has reduced the dimension of the membrane. The membrane wall thickness was not differing much after reaching the air gap of 30 cm. The membrane's average pore size and porosity increased with the increasing air gap of up to 50 cm. In terms of surface hydrophilicity, the trend showed improved surface hydrophilicity with the increasing air gap. Based on the results of PWP, BSA rejection, and SC, the optimum air gap was determined to be 50 cm. In conclusion, the ideal morphology for the hemodialysis membrane was achieved in this study.
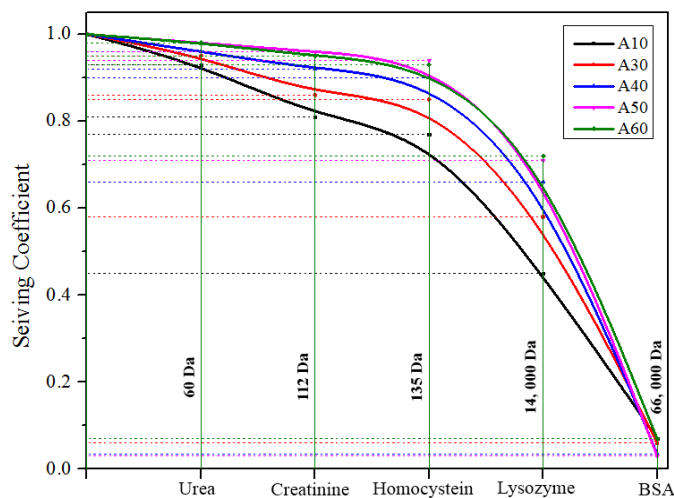
CRedit authorship contribution statement

N.Said: Data curation; Roles/Writing - original draft; Formal analysis.
S. Mansur: Investigation; Methodology; Validation.
M. N. Z. Abidin: Conceptualization; Supervision; Writing – review & editing.
A. F. Ismail: Funding acquisition.

Declaration of Competing Interest

The authors declare that they have no known competing financial interests or personal relationships that could have appeared to influence the work reported in this paper.

References

[1] N. Said, W.J. Lau, Y.C. Ho, S.K. Lim, M.N. Zainol Abidin, A.F. Ismail, A review of commercial developments and recent laboratory research of dialyzers and membranes for hemodialysis application, Membranes (Basel). 11 (2021) 1–38. doi:10.3390/membranes11100767.

[2] Y.A.H. Hakim, A.A. Abbas, A. Khalil, T.H. Ibrahim, A. Mustafa, Y.A.H. Hakim, I.J. Med, R. Health, The effect of hemodialysis on hemoglobin concentration, platelets count and white blood cells count in end-stage renal failure, Int. J. Med. Res. Health Sci. 5 (2016) 22–35.

[3] K. Ma, M.A. Khan, A. Hussain, Haemodialysis Membranes: A Review, J Membr Sci Technol. 9 (2019) 1–9.

[4] Y. Liu, Q. Han, T. Li, J. Hua, F. Liu, Q. Li, G. Deng, Heparin reduced dialysis through a facile anti-coagulant coating on flat and hollow fiber membranes, J. Memb. Sci. 595 (2020) 117593. doi:10.1016/j.memsci.2019.117593.

[5] G. Ankawi, W. Fan, D. Pomarè Montin, A. Lorenzin, M. Neri, C. Caprara, M. De Cal, C. Ronco, A new series of sorbent devices for multiple clinical purposes: current evidence and future directions, Blood Purif. 47 (2019) 94–100. doi:10.1159/000493523.

[6] M.K. van Gelder, J.A.W. Jong, L. Folkertsma, Y. Guo, C. Blüchel, M.C. Verhaar, M. Odijk, C.F. Van Nostrum, W.E. Hennink, K.G.F. Gerritsen, Urea removal strategies for dialysate regeneration in a wearable artificial

kidney, Biomaterials. 234 (2020) 119735. doi:10.1016/j.biomaterials.2019.119735.

[7] I. Baldwin, M. Baldwin, N. Fealy, M. Neri, F. Garzotto, J.C. Kim, A. Giuliani, F. Basso, F. Nalesso, A. Brendolan, C. Ronco, Concurrent versus counter-current dialysate flow during CVVHD. A comparative study for creatinine and urea removal, Blood Purif. 41 (2016) 171–176. doi:10.1159/000441270.

[8] S. Mansur, M.H.D. Othman, M.N.Z. Abidin, A.F. Ismail, S.H.S. Abdul Kadir, P.S. Goh, H. Hasbullah, B.C. Ng, M.S. Abdullah, R. Mustafar, Enhanced adsorption and biocompatibility of polysulfone hollow fibre membrane via the addition of silica/alpha-mangostin hybrid nanoparticle for uremic toxins removal, J. Environ. Chem. Eng. 9 (2021) 106141. doi:10.1016/j.jece.2021.106141.

[9] Q.F. Alsalhy, H.A. Salih, S. Simone, M. Zablouk, E. Drioli, A. Figoli, Poly(ether sulfone) (PES) hollow-fiber membranes prepared from various spinning parameters, Desalination. 345 (2014) 21–35. doi:10.1016/j.desal.2014.04.029.

[10] S. Mansur, M. Hafiz, D. Othman, A.F. Ismail, S. Hamimah, S. Abdul, F. Kamal, P.S. Goh, H. Hasbullah, B.C. Ng, M.S. Abdullah, Investigation on the effect of spinning conditions on the properties of hollow fiber membrane for hemodialysis application, J. Appl. Polym. Sci. 43633 (2016) 1–10. doi:10.1002/app.43633.

[11] R. Saghafi, M. Zarrebini, D. Semnani, The effect of bore fluid type on performance of treated polysulfone hollow-fiber membrane, Text. Res. J. 85 (2014) 281–293. doi:10.1177/0040517514521122.

[12] S. Mansur, M. Hafiz, D. Othman, A. Fauzi, M. Nidzhom, Z. Abidin, N. Said, P. Sean, H. Hasbullah, S. Hamimah, S. Abdul, Study on the effect of PVP additive on the performance of PSf / PVP ultrafiltration hollow fiber membrane, Malaysian J. Fundam. Appl. Sci. 14 (2018) 343–347.

[13] T.S. Chung, J.J. Qin, J. Gu, Effect of shear rate within the spinneret on morphology, separation performance and mechanical properties of ultrafiltration polyethersulfone hollow fiber membranes, Chem. Eng. Sci. 55 (2000) 1077–1091. doi:10.1016/S0009-2509(99)00371-1.

[14] F. Korminouri, M. Rahbari-Sisakht, T. Matsuura, A. F. Ismail, Surface modification of polysulfone hollow fiber membrane spun under different air-gap lengths for carbon dioxide absorption in membrane contactor system, Chem. Eng. J. 264 (2015) 453–461. doi:10.1016/j.cej.2014.11.110.

[15] Q. Zheng, P. Wang, Y. Yang, Rheological and thermodynamic variation in polysulfone solution by PEG introduction and its effect on kinetics of membrane formation via phase-inversion process, J. Memb. Sci. 279 (2006) 230–237. doi:10.1016/j.memsci.2005.12.009.

[16] A.F. Ismail, M.I. Mustaffar, R.M. Illias, M.S. Abdullah, Effect of dope extrusion rate on morphology and performance of hollow fibers membrane for ultrafiltration, Sep. Purif. Technol. 49 (2006) 10–19. doi:10.1016/j.seppur.2005.08.001.

[17] G.Q. Peng, Y.F. Wen, Y.G. Yang, L. Liu, W. Wang, Effect of dope extrusion rate on the formation and characterization of polyacrylonitrile nascent fibers during wet-spinning, Polym. Bull. 62 (2009) 657–666. doi:10.1007/s00289-009-0043-1.

[18] A. Ali, R.M. Yunus, M. Awang, A. Johari, R. Mat, Effect of shear rate on characteristics, performance and morphology of polysulfone blend membranes, Appl. Mech. Mater. 699 (2014) 305–310. doi:10.4028/www.scientific.net/AMM.699.305.

[19] P.S. Goh, B.C. Ng, W.J. Lau, A.F. Ismail, Inorganic nanomaterials in polymeric ultrafiltration membranes for water treatment, Sep. Purif. Rev. 44 (2015) 216–249. doi:10.1080/15422119.2014.926274.

[20] M.N.Z. Abidin, P.S. Goh, A.F. Ismail, M.H.D. Othman, H. Hasbullah, N. Said, S.H.S.A. Kadir, F. Kamal, M.S. Abdullah, B.C. Ng, Development of biocompatible and safe polyethersulfone hemodialysis membrane incorporated with functionalized multi-walled carbon nanotubes, Mater. Sci. Eng. C. 77 (2017) 572–582. doi:10.1016/j.msec.2017.03.273.

[21] N. Said, H. Hasbullah, M. Nidzhom, Z. Abidin, A.F. Ismail, P.S. Goh, M. Ha, D. Othman, S. Hamimah, S. Abdul, F. Kamal, M.S. Abdullah, B.C. Ng, Facile modification of polysulfone hollow-fiber membranes via the incorporation of well-dispersed iron oxide nanoparticles for protein purification, J. Appl. Polym. Sci. 136 (2019) 1–11. doi:10.1002/app.47502.

[22] N. Said, H. Hasbullah, A. Fauzi, M. Nidzhom, The effect of air gap on the morphological properties of PSf / PVP90 membrane for hemodialysis application, Chem. Eng. Trans. 56 (2017) 1591–1596.

[23] N. Said, M. Nidzhom, Z. Abidin, H. Hasbullah, A.F. Ismail, P.S. Goh, M. Ha, D. Othman, M.S. Abdullah, B.C. Ng, S. Hamimah, S. Abdul, F. Kamal, Iron oxide nanoparticles improved biocompatibility and removal of middle molecule uremic toxin of polysulfone hollow fiber membranes, J. Appl. Polym. Sci. 48234 (2019) 1–13. doi:10.1002/app.48234.

[24] G.J. Dahe, R.S. Teotia, S.S. Kadam, J.R. Bellare, The biocompatibility and separation performance of antioxidative polysulfone/vitamin E TPGS composite hollow fiber membranes, Biomaterials. 32 (2011) 352–365. doi:10.1016/j.biomaterials.2010.09.005.

[25] M.N.Z. Abidin, P.S. Goh, A.F. Ismail, M.H.D. Othman, H. Hasbullah, N. Said, S.H.S.A. Kadir, F. Kamal, M.S. Abdullah, B.C. Ng, Antifouling polyethersulfone hemodialysis membranes incorporated with poly (citric acid) polymerized multi-walled carbon nanotubes, Mater. Sci. Eng. C. 68 (2016) 540–550. doi:10.1016/j.msec.2016.06.039.

[26] R. Saghafi, M. Zarrebini, D. Semnani, The effect of bore fluid type on performance of treated polysulfone hollow fiber membrane, Text. Res. J. 85 (2014) 281–293. doi:10.1177/0040517514521122.

[27] A. Hedayat, J. Szpunar, N.A.P.K. Kumar, R. Peace, H. Elmoselhi, A. Shoker, Morphological characterization of the Polyflux 210H hemodialysis filter pores, Int. J. Nephrol. 2012 (2012) 1–6. doi:10.1155/2012/304135.

[28] A. Abdelrasoul, H. Doan, A. Lohi, C.-H. Cheng, Morphology control of polysulfone membranes in filtration processes: a critical review, ChemBioEng Rev. 2 (2015) 22–43. doi:10.1002/cben.201400030.

[29] A.C. Yamashita, K. Sakurai, —Physicochemical structures and features, in: Updat. Hemodial., 2015: pp. 163–189.

[30] M. Khayet, The effects of air gap length on the internal and external morphology of hollow fiber membranes, Chem. Eng. Sci. 58 (2003) 3091–3104. doi:10.1016/S0009-2509(03)00186-6.

[31] M. Irfan, A. Idris, N.M. Yusof, N.F.M. Khairuddin, H. Akhmal, Surface modification and performance enhancement of nano-hybrid f-MWCNT/PVP90/PES hemodialysis membranes, J. Memb. Sci. 467 (2014) 73–84. doi:10.1016/j.memsci.2014.05.001.

[32] X. Yu, L. Shen, Y. Zhu, X. Li, Y. Yang, W. Wang, M. Zhu, B.S. Hsiao, High performance thin-film nanofibrous composite hemodialysis membranes with efficient middle-molecule uremic toxin removal, J. Memb. Sci. 523 (2017) 173–184. doi:10.1016/j.memsci.2016.09.057.